J. Fluid Mech. (1987), *vol.* 179, *pp.* 383–405
Printed in Great Britain

Vortex induction and mass entrainment in a small-aspect-ratio elliptic jet

By CHIH-MING HO AND EPHRAIM GUTMARK
Department of Aerospace Engineering, University of Southern California, Los Angeles, CA 90089, USA

(Received 17 December 1985 and in revised form 21 October 1986)

A passive technique of increasing entrainment was found by using a small-aspect-ratio elliptic jet. The entrainment ratio of an elliptic jet was several times greater than that of a circular jet or a plane jet. The self-induction of the asymmetric coherent structure caused azimuthal distortions which were responsible for engulfing large amounts of surrounding fluid into the jet. In an elliptic jet, an interesting feature in the initial stability process is that the thickness of the shear layer varies around the nozzle. The data indicated that instability frequency was scaled with the thinnest initial momentum thickness which was associated with the maximum vorticity. Turbulence properties were also examined and were found to be significantly different in the major- and minor-axis planes.

1. Introduction

Jets are common configurations used in various mixing and thrust producing devices and several extensive investigations have been made on axisymmetric jets (e.g. Wygnanski & Fiedler 1969; Crow & Champagne 1971) and plane jets (e.g. Heskestad 1965). The two-dimensional characteristics of these two types of nozzles made experimental measurements and theoretical analyses much easier.

Studies on three-dimensional jets (elliptic or rectangular nozzles) have not been completely neglected but certainly have been very scarce. In the past, Sforza, Steiger & Trentacoste (1966), Komatsu (1969) and Sfeir (1978) have documented the velocity fields of three-dimensional jets. The most interesting discovery was the phenomenon of axis switching. Spreading in the minor-axis plane (the plane containing the minor axis of the nozzle) was much greater than that in the major-axis plane. Some distance downstream from the nozzle the cross-section of the jet eventually switched its orientation. The distance from the nozzle to the cross-over point was found to be a linear function of the aspect ratio (Krothapalli, Baganoff & Karamcheti 1981). The axis switch has also been found in isolated elliptic vortex rings (Viets & Sforza 1972; Dhanak & De Bernardinis 1981), and is due to the self-induction caused by vorticity distributed on an asymmetric contour.

When a jet is used in the mixing process or for thrust augmentation, a large mass entrainment, especially near the nozzle, is desired. The entrainment in a two-dimensional flow is dominated by vortex merging (Winant & Browand 1974; Ho & Huerre 1984). It also has been found that several active forcing methods are effective in manipulating vortex merging in plane mixing layers (Ho & Huang 1982; Oster & Wygnanski 1982), and in circular jets (Reynolds & Bouchard 1981). In previous three-dimensional-jet studies, the entrainments were not significantly different from those in two-dimensional flows (Trentacoste & Sforza 1967), but the jet aspect ratios

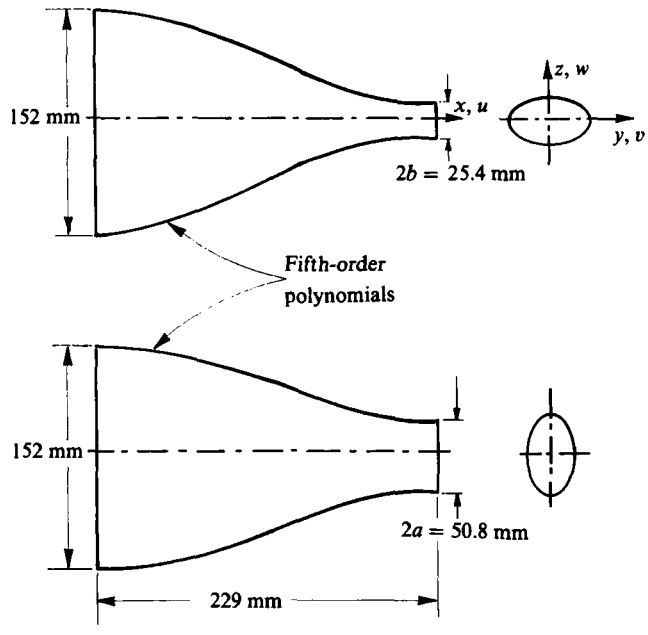

FIGURE 1. Sketch of the elliptic nozzle.

were 5:1 or larger. We started to investigate an elliptic jet with an aspect ratio of 2:1. The mass entrainment before the end of the potential core was found to be three to eight times (depending on the axial locations) higher than that in an axisymmetric or a two-dimensional jet. When the results were first presented (Ho & Gutmark 1982; Gutmark & Ho 1982), we suggested that a three-dimensional nozzle with a small aspect ratio could be a very effective passive control device for enhancing mass entrainment near the nozzle exit. In this paper, the mass entrainment and its mechanism in an elliptic jet are discussed, the instability process is studied and finally the turbulence properties in the major- and minor-axis planes are documented.

2. Experimental set-up

The air jet was driven by an axial fan. Air passed through a 7° diffuser into a cylindrical stagnation chamber. Inside the diffuser and the stagnation chamber, screens, foam rubber and honeycomb were used to reduce the turbulence level to 0.4% at the nozzle exit. The contraction changed from a circular cross-section, 152 mm in diameter, to an elliptic nozzle. The major diameter of the nozzle $2a$ was 50.8 mm and the minor diameter $2b$ was 25.4 mm. The contraction contours in the two axis planes were fifth-order polynomials (figure 1). A hydraulic diameter D_h = (4 × nozzle area/perimeter) and the value of a are used as scales for normalization.

Single hot-wire and x-wire probes were used to measure the mean and turbulent velocities. The hot wire was made of a 2.5 μm Pt–Rd wire and the frequency response of the constant-temperature anemometer was 30 KHz. By placing the probe at the centre of the nozzle exit plane, the single hot wire was calibrated against the mean jet speeds which were measured by a Baratron pressure transducer (type 270). The transducer output had 0.001% linearity and long time stability. The output of the

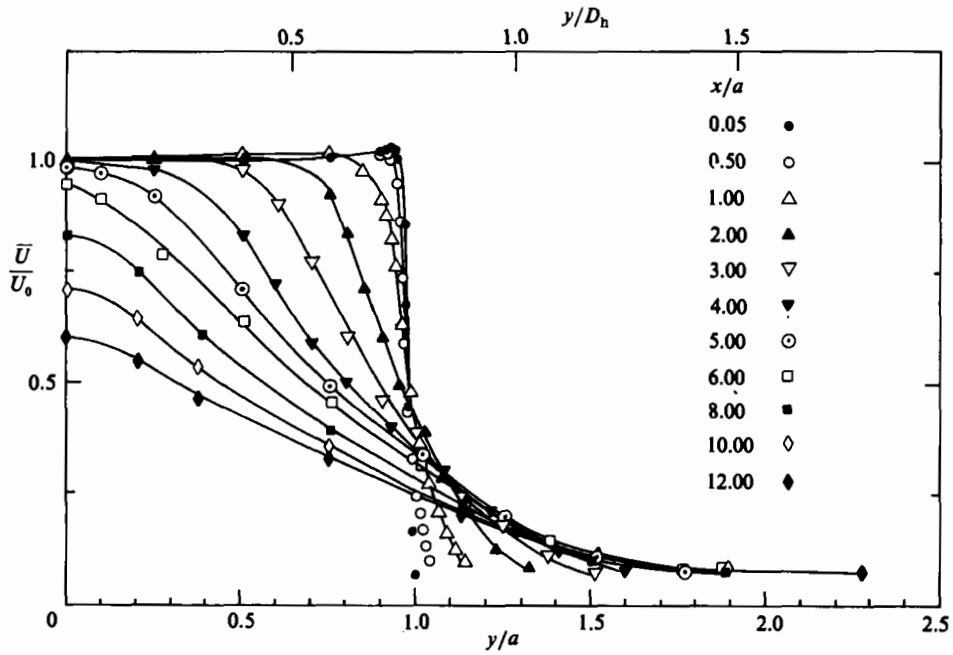

FIGURE 2. Mean axial velocity profiles in the major-axis plane.

hot wire was used to fit a power law which led to the determination of the constants in King's Law. When the x-wire was calibrated, an angular displacement mechanism was used such that the x-wire could be rotated with respect to the mean-flow direction and always remain at the centre of the nozzle exit. The probe was mounted on a three-dimensional traverse which has a spatial resolution of 6.35×10^{-4} cm.

The flow field was measured at a Reynolds number of 78000 based upon the major diameter and the jet exit speed ($U_0 = 21.9$ m/s). In a typical survey across the shear layer, ten to twenty sampling points were used. At each measuring point, the length of the data record was approximately equal to 5000 periods of the passing coherent structures. This long record ensured statistical stability for data analysis. The data were digitized and processed by an on-line computer (PDP 11/55). The FFT was performed by a AP-120B array processor which was interfaced with the computer.

3. Mean-velocity field

3.1. *The mean axial velocity*

The exit velocity profiles were almost uniform in the two axis planes (figures 2 and 3). A slight overshoot of the velocity (about 2 % of the centreline exit speed U_0) existed near the wall. The top-hat profiles eventually evolved into bell-shaped distributions. The potential core ended at about $x/a = 5$ (figure 4) and the decay of the centreline velocity $\overline{U}_c$ was inversely proportional to the streamwise distance downstream from the potential core.

The spreading in the two axis planes was noticeably different. In the major-axis plane, the shear layer mainly spread into the potential core (figure 2), while the shear layer spread widely into the quiescent surroundings in the minor-axis plane (figure 3). It is interesting to note that the differences of the near-field pressure

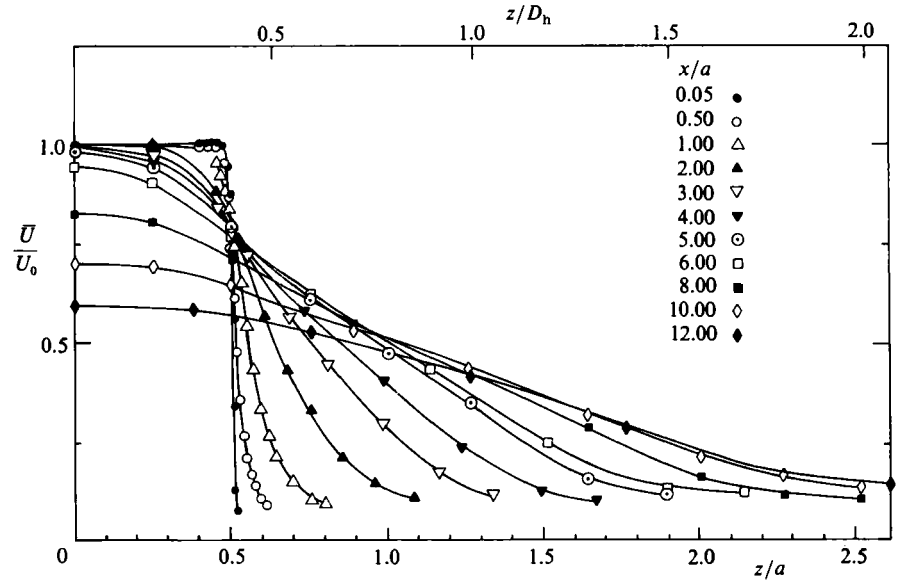

FIGURE 3. Mean axial velocity profiles in the minor-axis plane.

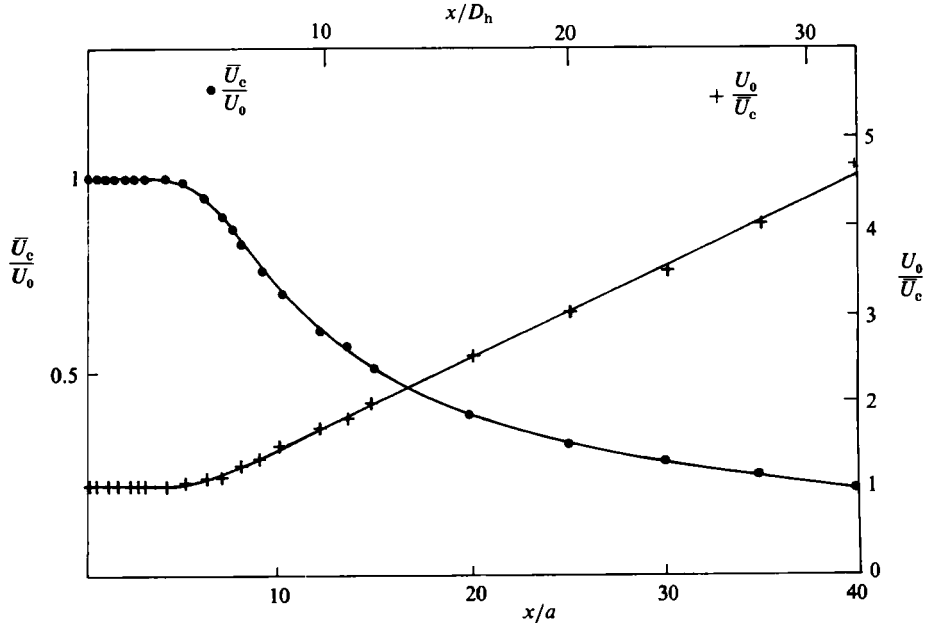

FIGURE 4. Decay of mean centreline velocity.

fluctuations in the two axis planes are not very appreciable (Gutmark & Ho 1985), because pressure represents a volume integral of the fluctuating quantities around the measuring point. The geometry of the jet cross-section is shown in figure 5 by plotting the jet width at $\overline{U}/\overline{U}_c = 0.5$. The jet grew almost linearly in the minor-axis plane. The jet width in the major-axis plane remained constant or slightly decreased until $x/a \approx 13$, then it began growing. Three axis switches were observed within the

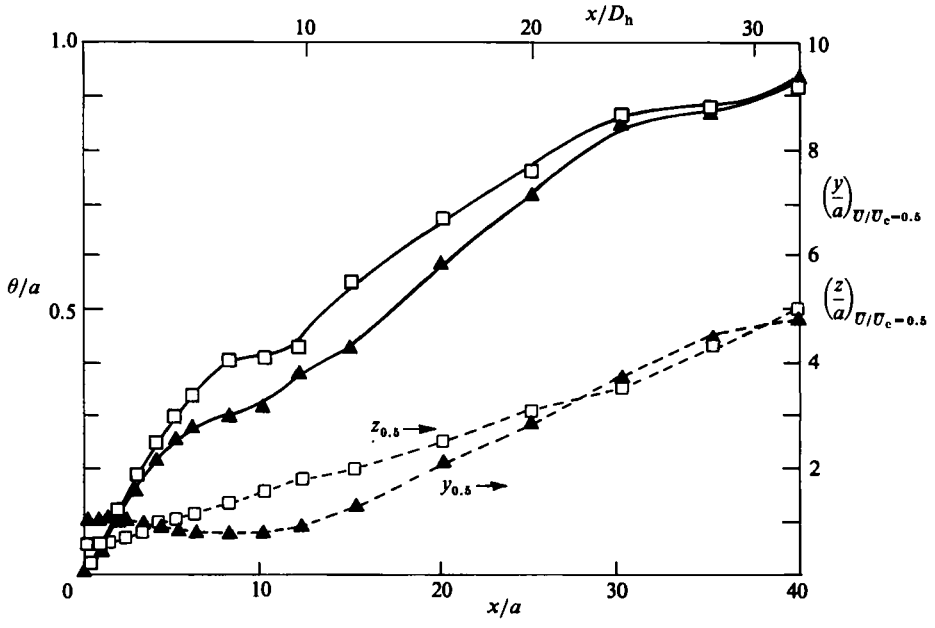

FIGURE 5. The jet width and the momentum thickness as a function of streamwise distance: θ/a (——); $(y/a)_{U/U_c=0.5}$, $(z/a)_{U/U=0.5}$ (------). ▲, Major axis; □, minor axis.

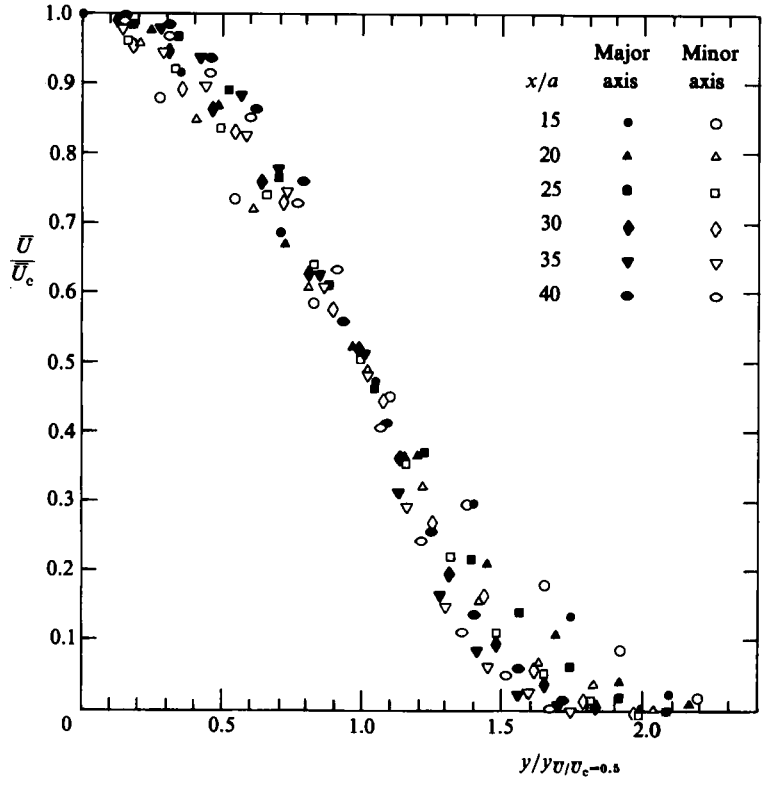

FIGURE 6. Velocity profiles ($15 < x/d < 40$) normalized by half-jet width.

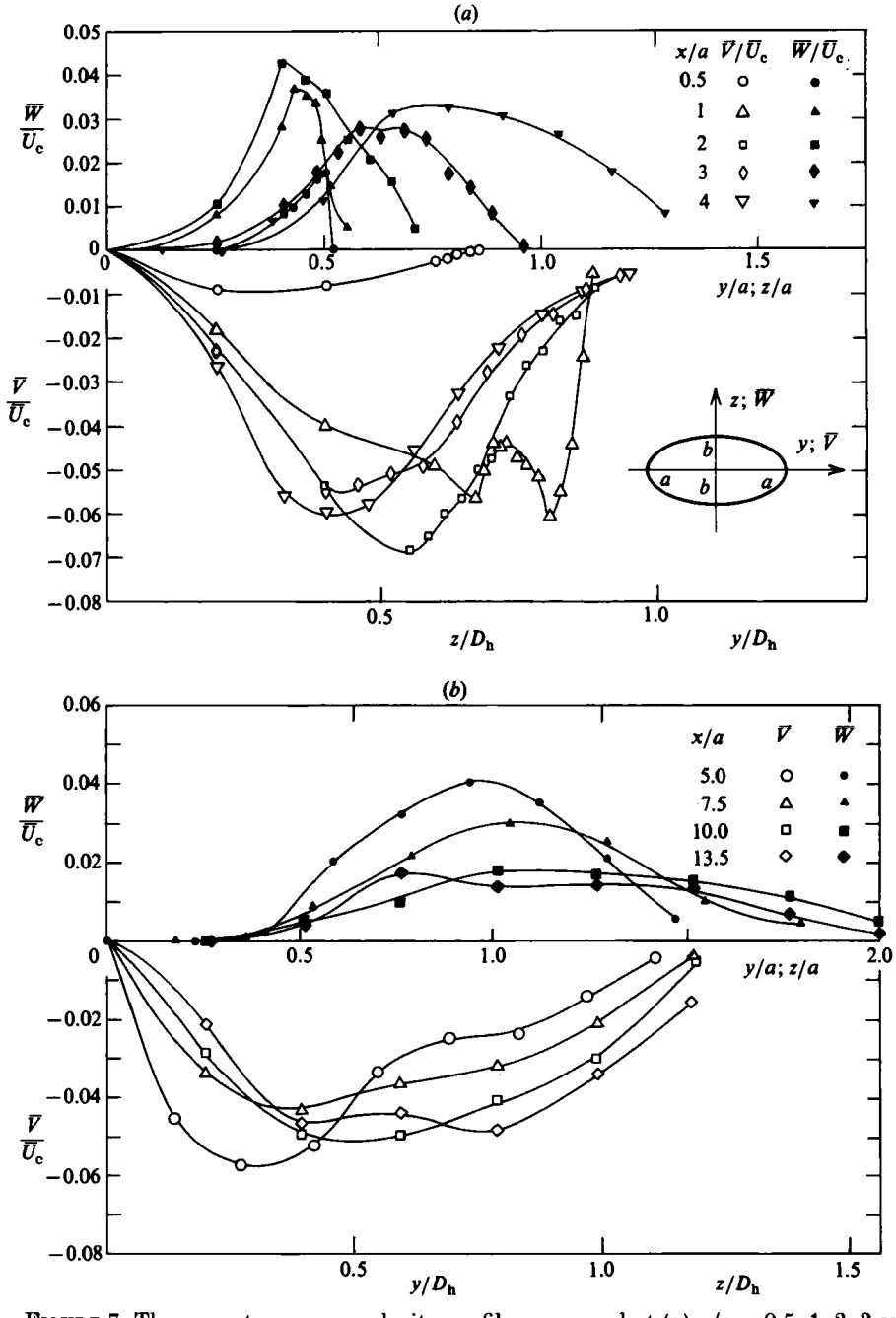

FIGURE 7. The mean transverse velocity profiles measured at (*a*) $x/a = 0.5$, 1, 2, 3 and 4; (*b*) $x/a = 5$, 7.5, 10 and 13.15.

measuring range $x/a \leqslant 40$. The first switching occurred at $x/a \approx 5$ which followed the scaling trend with respect to the aspect ratio (Krothapalli *et al.* 1981). The jet had not reached a circular cross-section by $x/a = 40$. In the range of $15 \leqslant x/a \leqslant 40$, the velocity profiles did not collapse by normalizing to the local half-jet width (figure 6).

The initial momentum thickness θ_0 was 0.168 mm in the major-axis plane and 0.134 mm in the minor-axis plane. In a very short distance downstream from the nozzle, the momentum thickness in the minor-axis plane became thicker than that in the major-axis plane (figure 5); this trend continued until $x/a \approx 38$. The growth rates of the momentum thicknesses decreased substantially where the axis switching occurred at $x/a \approx 5$ and 28 (figure 5). In both axis planes, the growth rates near the nozzle, $x/a < 5$, were about eight times greater than the growth rates at downstream, $30 < x/a < 40$.

3.2. *The mean transverse velocities*

The mean transverse velocities $\overline{V}$ and $\overline{W}$ were measured from $x/a = 0.5$ to 13.5 (figure 7*a*, *b*). Further downstream from $x/a = 13.5$ the accuracy of measuring $\overline{V}$ and $\overline{W}$ became questionable, because $\overline{V}$ and $\overline{W}$ would be less than one percent of the axial velocity component. In the major-axis plane, the jet width did not increase for $x/a < 13$ (figure 5). This was also indicated by $\overline{V}$ which had a negative value (figure 7*a*, *b*). In the minor-axis plane, the jet width spread from the nozzle exit (figure 5) and the values of $\overline{W}$ were always positive. Near the jet axis, the values of $\overline{W}$ were very small. For $3.0 \leqslant x/a \leqslant 13.5$, $\overline{W}$ was equal to zero for $z/a \leqslant 0.25$.

4. The instability process

4.1. *The lengthscales*

In a two-dimensional mixing layer, an axisymmetric jet or a plane jet, the initial momentum thickness is uniform along the trailing edge of the nozzle or the splitter plate. The instability frequency in such flows was found to be scaled with the ratio of the velocity to the momentum thickness (Michalke 1965; Monkewitz & Huerre 1982; Michalke & Hermann 1982). The ratio is a measure of the mean vorticity. A special feature of this elliptic jet is that the momentum thickness varies continuously around the nozzle. The development of instability waves in a shear layer with a non-uniform lengthscale is a very interesting and practically unknown problem.

The spectrum measured near the nozzle of the elliptic jet showed two clear peaks (figure 8): one was the fundamental f_0 and the other was the subharmonic. The peak frequencies of the spectra measured around the nozzle have constant values for the fundamental and the first subharmonic. The results suggest that a single ring vortex will shed from the nozzle in an instant. The non-uniform lengthscale does not greatly affect the topology of the vortex structures. The initial Strouhal number based upon the momentum thickness is 0.0165 in the minor-axis plane and 0.0207 in the major-axis plane.

The linear stability analysis of an elliptic jet was first performed by Crighton (1974) for a large-aspect-ratio case. Morris & Miller (1984) studied the instability in a small-aspect-ratio elliptic jet. They investigated the amplification rates of the instability waves. Four modes (ce_0, se_1, ce_1 and se_2) were discussed, where ce_0 is a mode symmetric to both axes, se_1 is symmetric to the major axis, ce_1 is a mode symmetric to the minor axis and se_2 is symmetric to the origin. The most amplified frequencies of the ce_0 mode were found to be scaled with the thinner momentum thickness in the two axis planes and the Strouhal number was 0.017; this is very close to the measured value, 0.0165, in the minor-axis plane which has a thinner momentum thickness. *The experimental and the theoretical results indicate that the instability in the elliptic jet with non-uniform initial momentum thickness is mainly determined by the maximum vorticity which is associated with the smallest momentum thickness.*

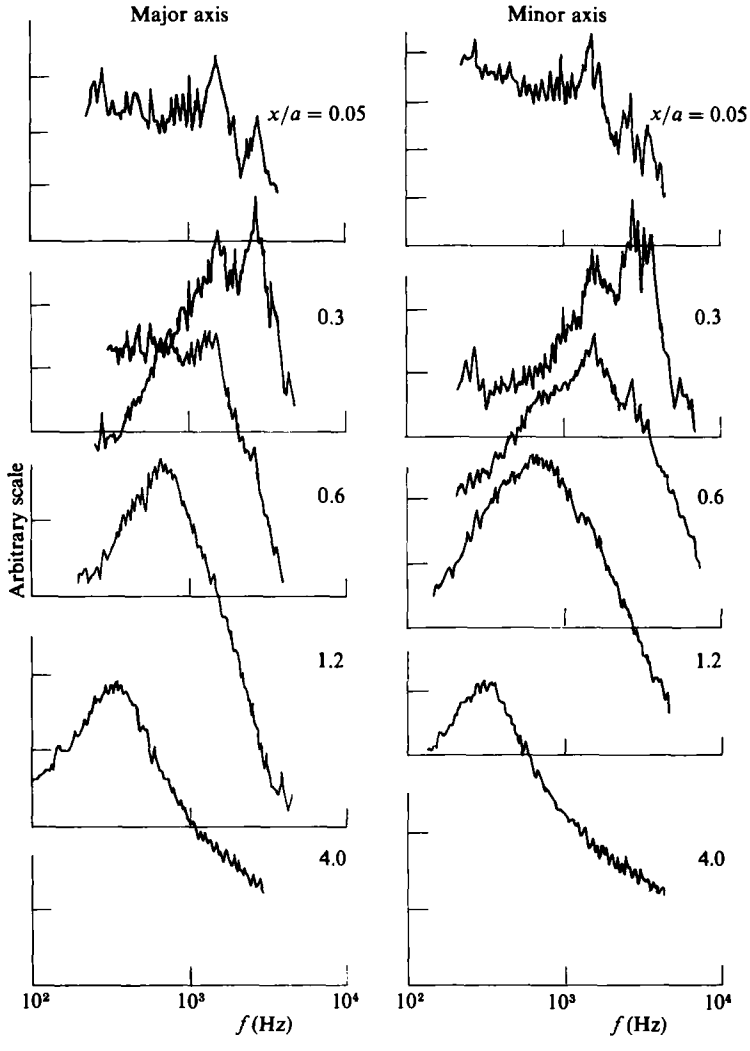

FIGURE 8. Spectra measured at $\bar{U}/U_0 = 0.5$.

4.2. *The eigenfunctions and the amplification of instability waves*

Near the nozzle, $x/a \leqslant 0.3$, the eigenfunctions of the fundamental have double peaks in both the major- and the minor-axis planes (figures 9 and 10); y_M is where the eigenfunction has its maximum value. The minimum of the eigenfunction occurred at about one initial momentum thickness θ_0 away from the high peak at the low-speed side. At the same radial position, the phase variation experienced a phase jump of π (figure 11). The open symbols in figures 9 and 10 are the eigenfunctions predicted from stability theory (S. Koshigoe 1986, private communication). The shape and the location of the minimum value were well predicted. Further downstream, $x/a \geqslant 1.2$, the eigenfunctions became single-peak curves.

The subharmonic eigenfunction had only one peak before $x/a < 0.5$ (figure 12). After the fundamental reached its maximum amplitude, $x/a > 0.5$ (figure 13), the

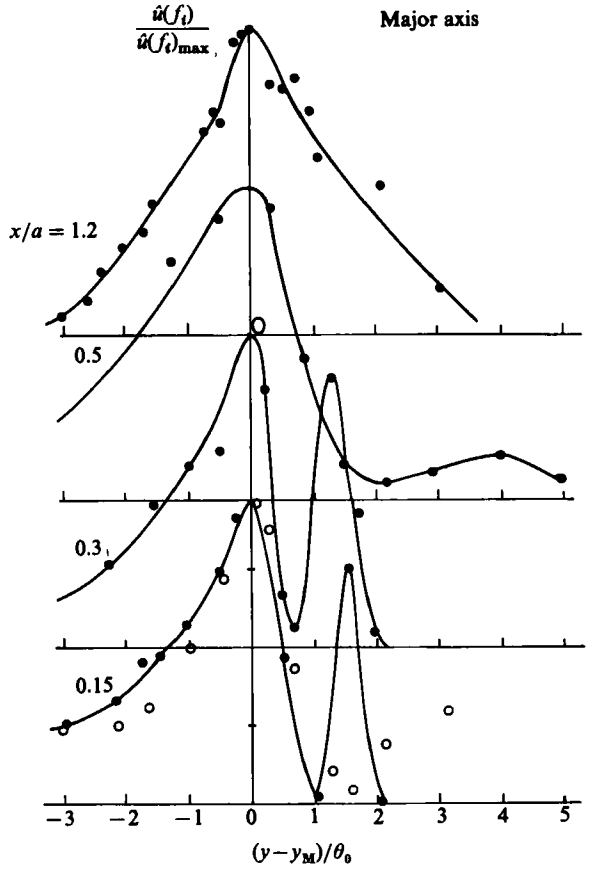

FIGURE 9. The eigenfunctions of the fundamental in the major-axis plane: O, calculated eigenfunction (S. Koshigoe 1986, private communication)

x/a	y_M/θ_0
0.15	0.94
0.3	0.935
0.5	0.919
1.2	0.901

eigenfunctions became double-peak curves (not shown here) and followed the same evolutionary trend as the fundamental.

The instability waves grew exponentially with streamwise distance. The amplification of the waves was obtained by integrating the eigenfunctions across the shear layer; it was then normalized by the jet exit velocity and the initial momentum thickness:

$$E(f) = \frac{1}{2\theta_0}\int_0^\infty \left(\frac{u'(f)}{U_0}\right)^2 \mathrm{d}y.$$

The fundamental first peaked at $x/a \approx 0.5$ (figure 13). The first subharmonic amplified at a slower rate and peaked at $x/a \approx 0.6$. At about twice the distance, $x/a \approx 1.2$, the second subharmonic had its maximum value of $E(f)$.

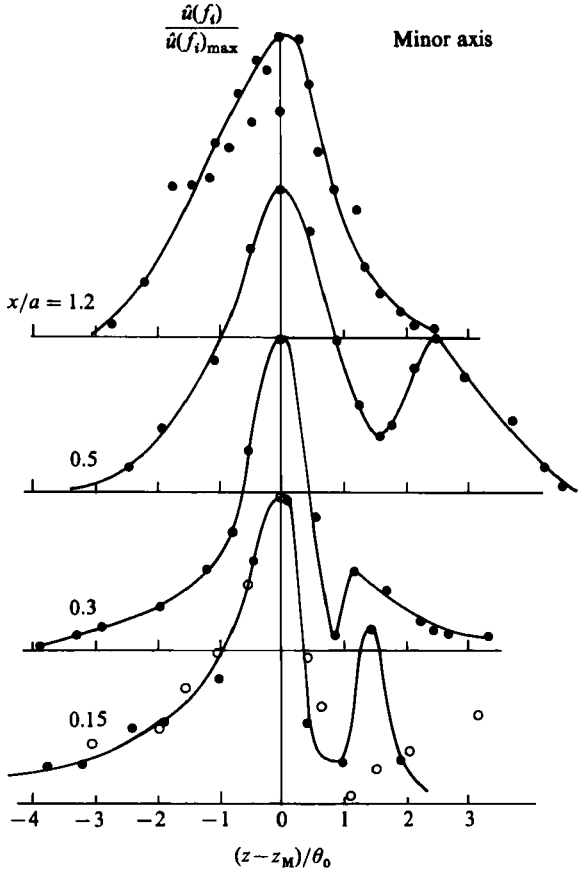

FIGURE 10. The eigenfunctions of the fundamental in the minor-axis plane: ○, calculated eigenfunction (S. Koshigoe 1986, private communication)

x/a	z_M/θ_0
0.15	0.486
0.3	0.478
0.5	0.454
1.2	0.52

The amplification rates in the major- and the minor-axis planes were measured and normalized with the initial momentum thickness in each axis plane respectively (table 1). The normalized amplification rates were the same in both planes and their values were compared with the analytical results (Morris & Miller 1984; Koshigoe *et al.* 1986). The measured data agreed well with the calculated values of the ce_0 and the ce_1 modes, but did not match with values of the se_0 and the se_1 modes. We noticed that a mismatch also existed between the measured Strouhal number and the predicted values of the *se* modes.

4.3. *The merging of elliptical vortices*

In a two-dimensional mixing layer, it has been shown that the position of the vortex merging can be inferred from the peak location of the instability waves and needs four initial instability wavelengths to accomplish the first merging for the case of a

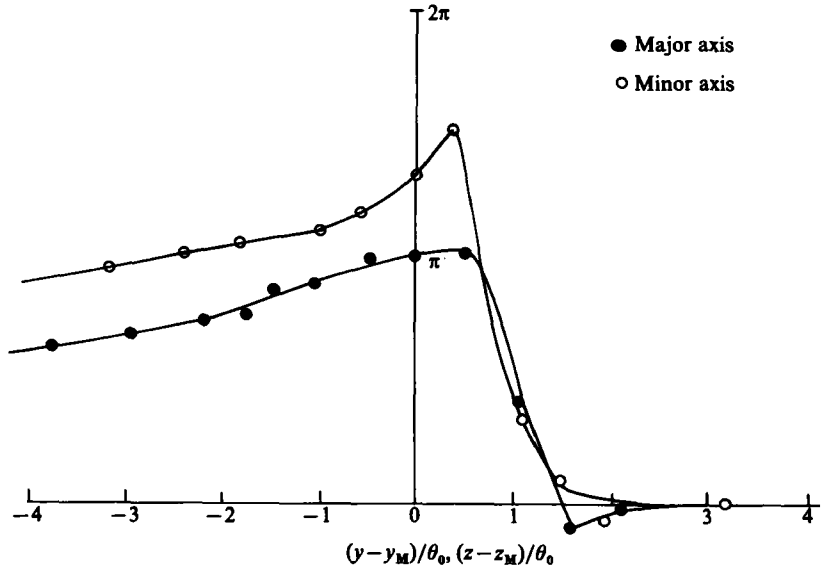

FIGURE 11. The phase variation of the fundamental across the shear layer at $x/a = 0.15$.

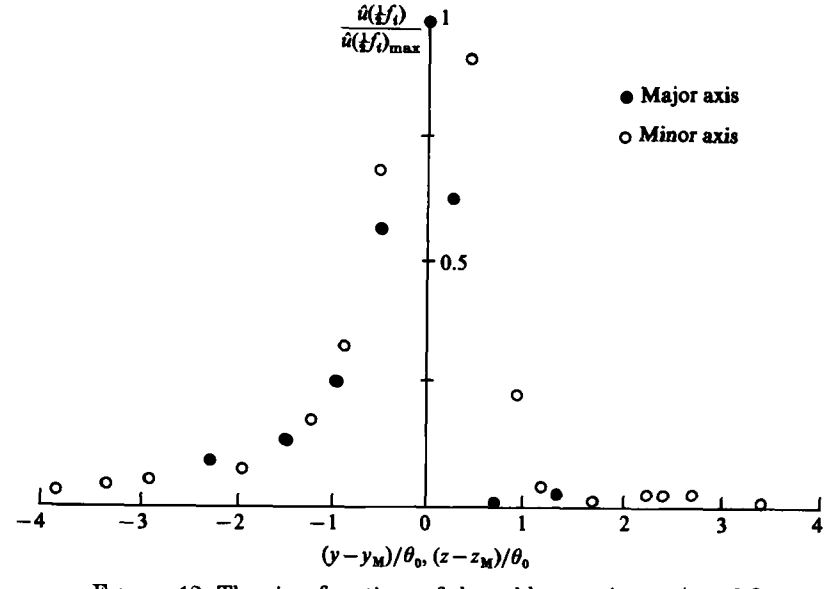

FIGURE 12. The eigenfunctions of the subharmonic at $x/a = 0.3$.

jet whose velocity ratio, $\Delta U/2\overline{U} = 1$ (Ho & Huang 1982). This finding is re-examined in an unforced elliptic jet. The variation of the peak frequencies of the spectra measured along the edge of the shear layer indicated the change of the passage frequencies of the structures (figure 14). Two discontinuities near $x/a = 0.6$ and 1.0, each with a frequency halving, corresponded to two successive pairing locations. The two positions were close to the peak regions of the first subharmonic and the second

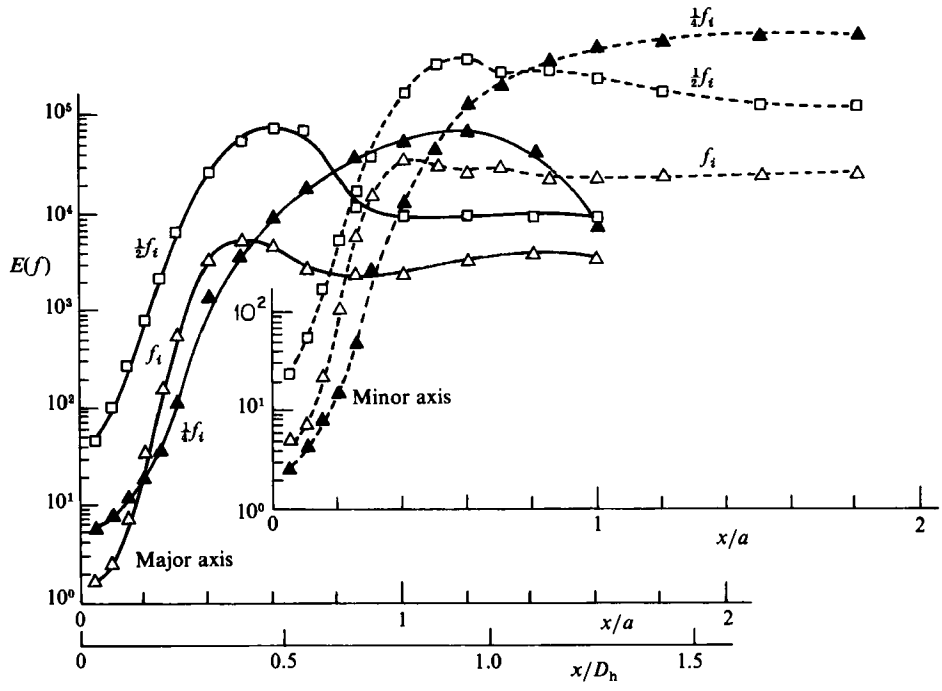

FIGURE 13. The amplification of the spectral components in the major- and the minor-axis planes.

	Major axis		Minor axis	
	f_1	$\frac{1}{2}f_1$	f_1	$\frac{1}{2}f_1$
Measured $(-\alpha\theta_0)_1$	0.089	0.067	0.088	0.058
ce_0 $(-\alpha\theta_0)_1$	0.089	0.05	0.089	0.05
ce_1 $(-\alpha\theta_0)_1$	0.089	0.05	0.089	0.05

TABLE 1. Measured and calculated amplification rates

subharmonic (figure 13). They were about equal to four and eight initial instability wavelengths, $\lambda_0 = U_0/2f_0 = 0.4$ cm, downstream from the trailing edge. We should note that the peak positions of the subharmonics in the major- and minor-axis planes are not exactly at the same position or are sometimes hard to define. This is probably due to the large azimuthal distortion which occurs during the vortex merging as has been observed in the dye-trace visualization experiment (Gutmark & Ho 1983, 1986, and figure 15*a*).

5. Mass entrainment and vortex induction

5.1. *Mass entrainment*

The jet entrains fluid from the surroundings and the total mass increases with streamwise distance. In many applications, large entrainment is required for better performance. In the past, *active control* of the vortex evolution process (Ho & Huang

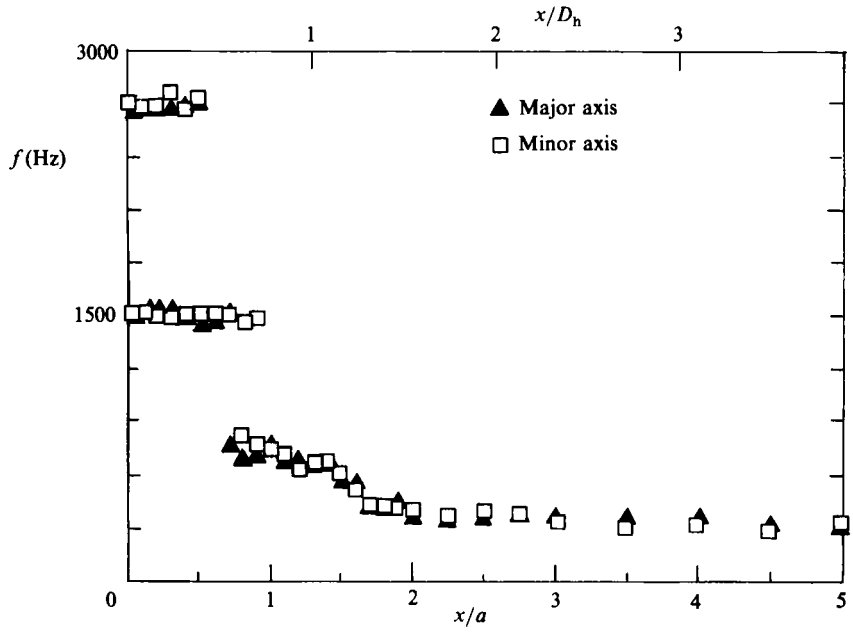

FIGURE 14. The peak frequencies of the spectrum measured along the shear layer.

1982; Oster & Wygnanski 1982; Lee & Reynolds 1985) was developed for this purpose. Now we find that a small-aspect-ratio elliptic jet can entrain several times more fluid than a circular or a plane jet. Most importantly, it is a *passive device*, which is more desirable in technical usage.

The cross-section of an elliptic jet changes its shape at various positions downstream from the nozzle. The mass flow rate cannot be measured only from velocity profiles in the two axis planes but has to be obtained by integrating the velocities across the whole cross-section. The constant-velocity contours are shown in figure 16 for several streamwise stations. At the first two stations, the jet still had the elliptical shape with the same orientation as the nozzle. The aspect ratio continued to decrease owing to larger spreading in the minor-axis plane. At $x/a = 5$, the cross-section became diamond shaped. In the case of an isolated elliptic ring (Viets & Sforza 1972; Dhanak & De Bernardinis 1981), it evolved into a diamond-shaped ring, but its axes had about a 45° difference in orientation from that in figure 16. The difference could be due to the vortex amalgamation in the elliptic jet. At $x/a = 10$, the axis switching was obvious.

The entrainment is defined as the difference between the mass flow rate at a station Q and at the nozzle exit Q_0. The entrainment ratios $(Q-Q_0)/Q_0$ of the elliptic jet (aspect ratio 2:1), the circular jet (aspect ratio 1:1) and the two-dimensional jet (aspect ratio 24:1) are plotted in figure 17. The increase of mass entrainment in an elliptic jet is phenomenal. The entrainment ratio measures the increase of mass flow in the jet stream (figure 17). The spreading of the momentum thickness indicates the growth of the momentum in the shear layer (figure 5). The growth rate in the minor-axis plane, 0.059, is about 20% larger than that in the major axis plane, 0.049. Both values are much higher than the growth rate, 0.032, of an axisymmetric jet at the same speed measured in the same facility with a circular nozzle.

After these results were first presented (Ho & Gutmark 1982; Gutmark & Ho 1982),

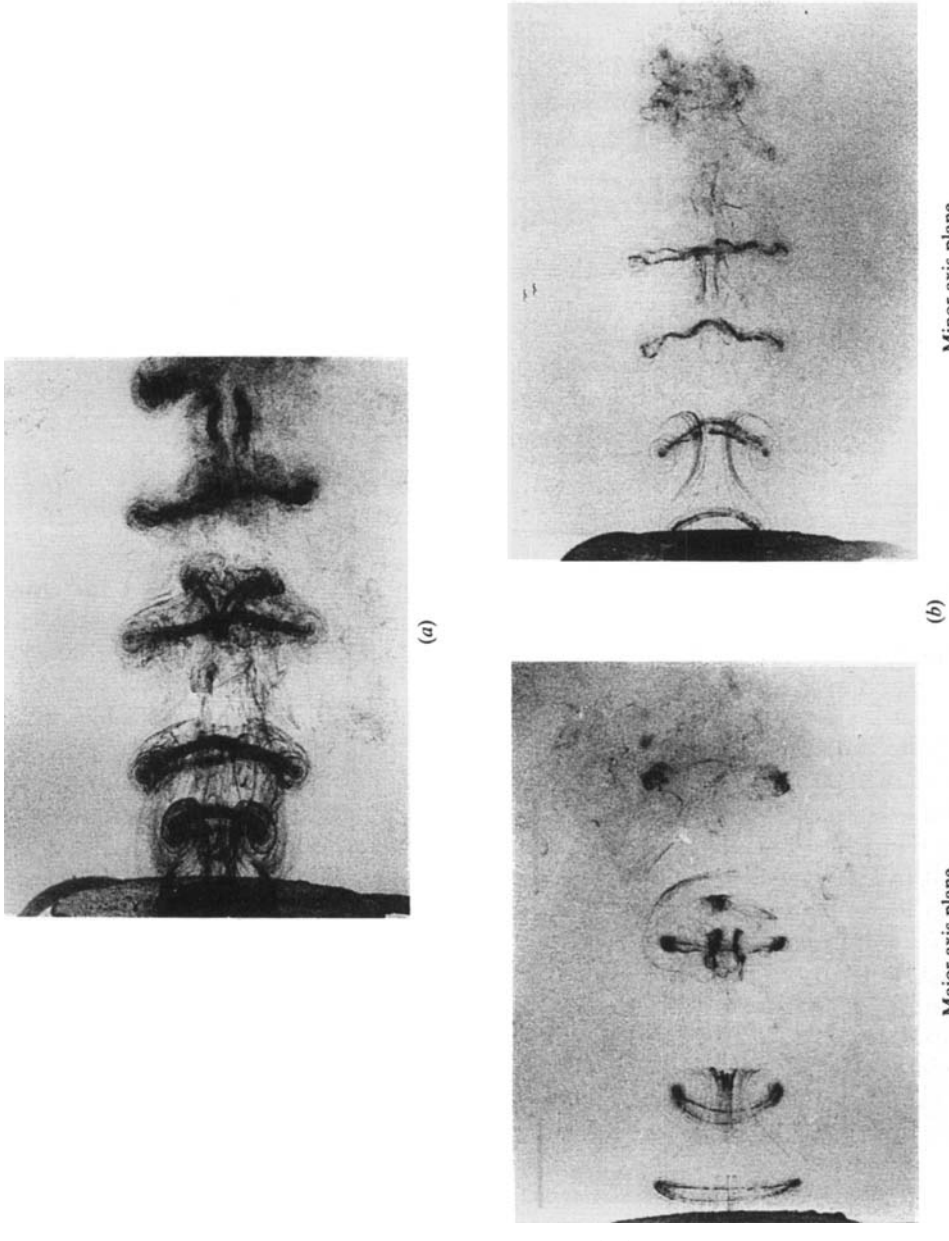

FIGURE 15. (a) Vortex merging (tagged by dye traces) in a forced elliptic jet. (b) Azimuthal deformation of vortex (tagged by dye traces) in a forced elliptic jet (Gutmark & Ho 1983, 1986).

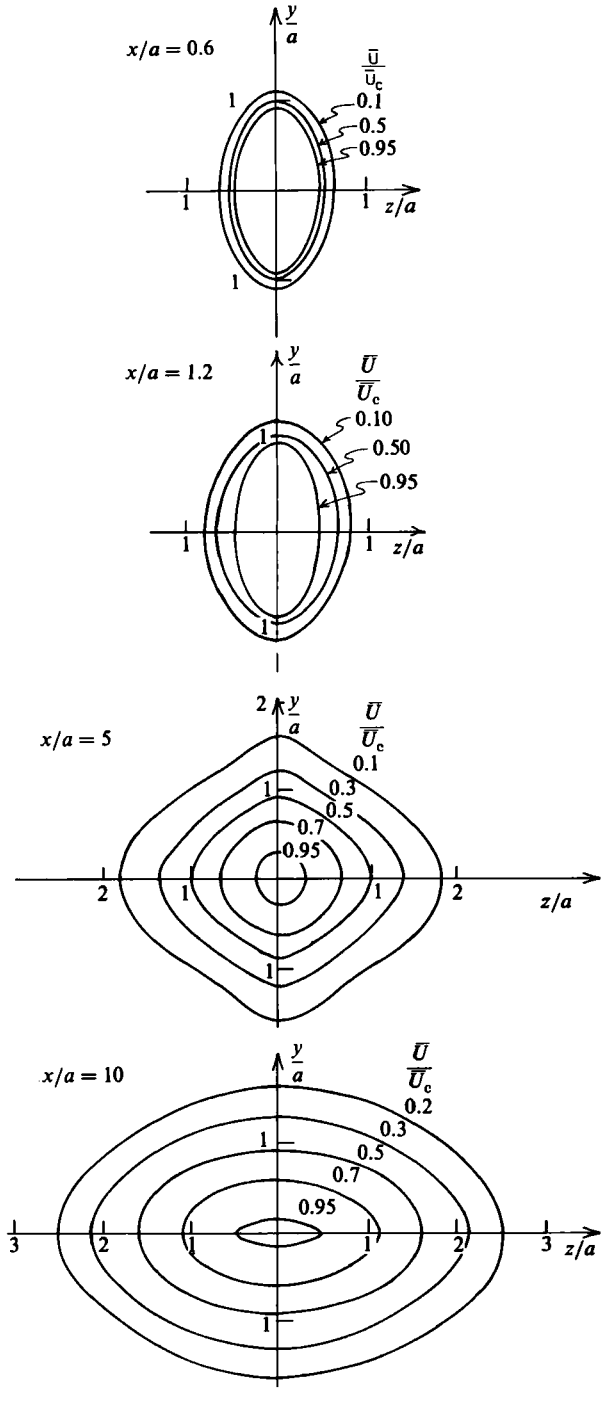

FIGURE 16. Constant-velocity contours.

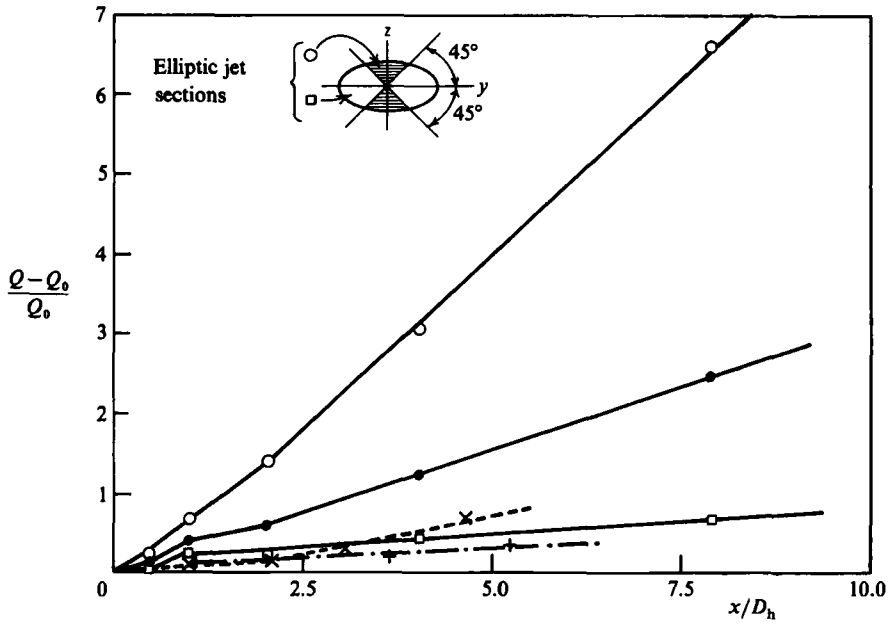

FIGURE 17. The entrainment ratio for an elliptic jet, hydraulic diameter $D_h = 3.23$ cm (●); a circular jet, $D_h = 3.81$ cm (×); and a two-dimensional jet, $D_h = 4.88$ cm (Ho & Hsiao 1982) (+).

there were several subsequent works on this subject. Husain & Hussain (1983) measured the half-width in the two axis planes. Unfortunately, it is impossible to confirm our findings regarding large mass entrainment with their data because of the lack of off-axis information. The aspect ratio is the obvious major parameter in determining the enhancement of the jet spreading, because large entrainment was not reported in previous three-dimensional-jet studies (Trentacoste & Sforza 1967) in which the aspect ratios were larger than 5:1. Schadow *et al.* (1984) made measurements in jets with several aspect ratios and suggested that the optimum value is between 2:1 and 3:1. They further showed that the centreline temperature of the flame from an elliptic nozzle reached an asymptotic value in a much shorter distance than that from a circular nozzle. This proves that much better fine-scale mixing occurs in an elliptic jet than in an axisymmetric jet.

5.2. *Vortex induction*

It was not clear what the main mechanism was for the phenomenal increase of the entrainment in the jet stream. This question was clarified by a simple estimation of the mass flow in two sections of the elliptic jet (figure 17); one section (the shaded portion) covers the area around the minor axis while the other covers the region containing the major axis. The mass entrainment of the two sections is plotted at several streamwise stations (figure 17). The large entrainment of the elliptic jet was found to be mainly produced in the portion near the minor axis. In the region near the major axis, the entrainment was approximately the same as that of the circular or the two-dimensional jet for $x < 5a$. This finding reveals a very efficient entrainment mechanism: *the self-induction of the vorticity distributed around an asymmetric*

contour azimuthally distorts the elliptic vortex ring, the portion of the vortex near the minor axis moves outward (see the dye-rings in figure 15b), a large amount of the surrounding fluid is then induced towards the axis and entrained into the jet.

In the past, the aspect ratios used in three-dimensional-jet studies were equal to or greater than 5:1, the azimuthal distortion took longer to evolve in the streamwise direction than that of a 2:1 aspect ratio jet (Krothapalli *et al.* 1981). When the distortion became appreciable, the vorticity was already very diffused. The entrained fluid induced by these diffused vortices would be much less and hence a large mass entrainment had not been observed.

The vortex arrangement in a jet or a mixing layer is not a stable formation. Owing to the mutual induction, two or more vortices will coalesce into a single structure. Winant & Browand (1974) have shown that entrainment in a two-dimensional shear layer takes place during the vortex merging event. Vortex merging occurs in an elliptic jet and the vortices deform azimuthally at the same time (figure 15*a*). The azimuthal deformation increases the interfacial area and engulfs more fluid from both streams into the mixing layer. Therefore, the spreading of the shear layer in an elliptic jet is faster than that in the two-dimensional flows.

Kibens & Wlezien (1985) used nozzles with indeterminate origins to generate non-circular vortices; large entrainment was also observed. Apparently, *the entrainment is always greatly facilitated by the asymmetry in vortical structures. The self-induction of these asymmetric vortices is a new class of entrainment mechanism.* Techniques, either passive or active, that can accentuate the asymmetry of the vortices will be able to promote the entrainment.

6. Turbulence properties

6.1. *Turbulence intensities*

Three components of the velocity fluctuations were measured in the major- and minor-axis planes. The centreline turbulence levels of all three components increased with x and reached peaks at $x/a = 10$ (figure 18) which was about twice the length of the potential core. In the case of the circular and two-dimensional jets, the peak of the centreline turbulence occurred at the end of the potential core. The distributions of the transverse velocities v' and w' were similar but their levels were lower than that of the streamwise component.

All the velocity fluctuations had a two-peak profile initially (figures 18–23), and evolved into a bell-shaped distribution after $x/a = 10$. In the major-axis plane, the location of the peak turbulence level shifted towards the jet axis with increasing streamwise distance. In the minor-axis plane, the peak position shifted away from the jet axis and the spread of the curve was much wider than that in the major-axis plane. A large part of the fluctuating velocity was contributed by the large coherent structures (Browand & Ho 1983). Therefore, the shifting of the peaks reflected the azimuthal distortion of the elliptic vortex.

The value of maximum u' increased with streamwise distance (figures 18 and 19) until $x/a = 1.0$ but started to decline after $x/a > 1.0$; $x = a$ is the region where the second vortex merging occurred (figure 14). The same trend in the streamwise variation was found for the maximum v' in the major-axis plane and maximum w' in the minor-axis plane. The peak values of these three fluctuation levels were about the same, $0.2U_0$. The v' in the minor-axis plane and w' in the major-axis plane were

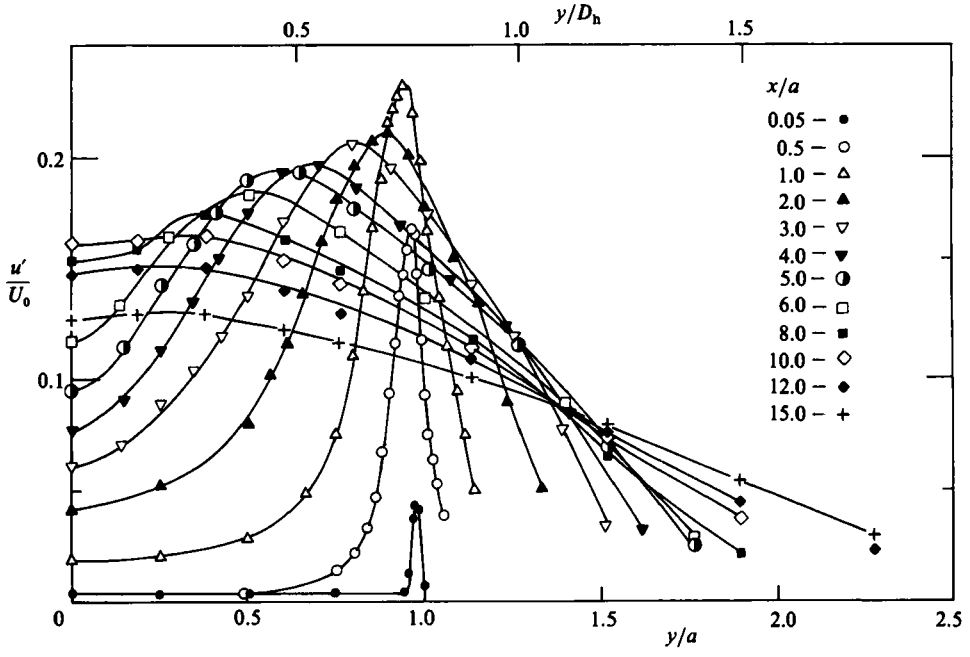

FIGURE 18. The u'-profiles in the major-axis plane.

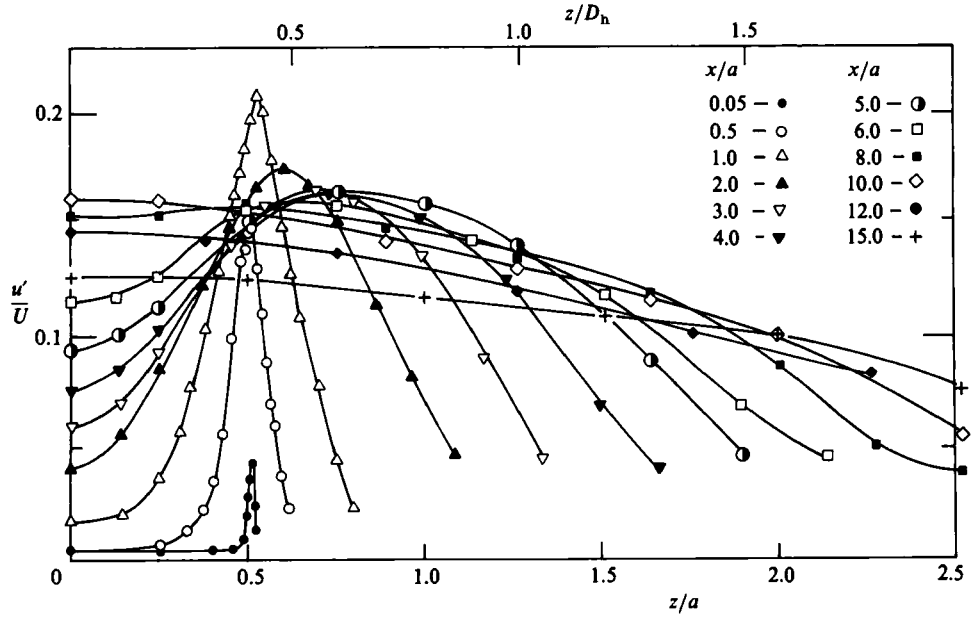

FIGURE 19. The u'-profiles in the minor-axis plane.

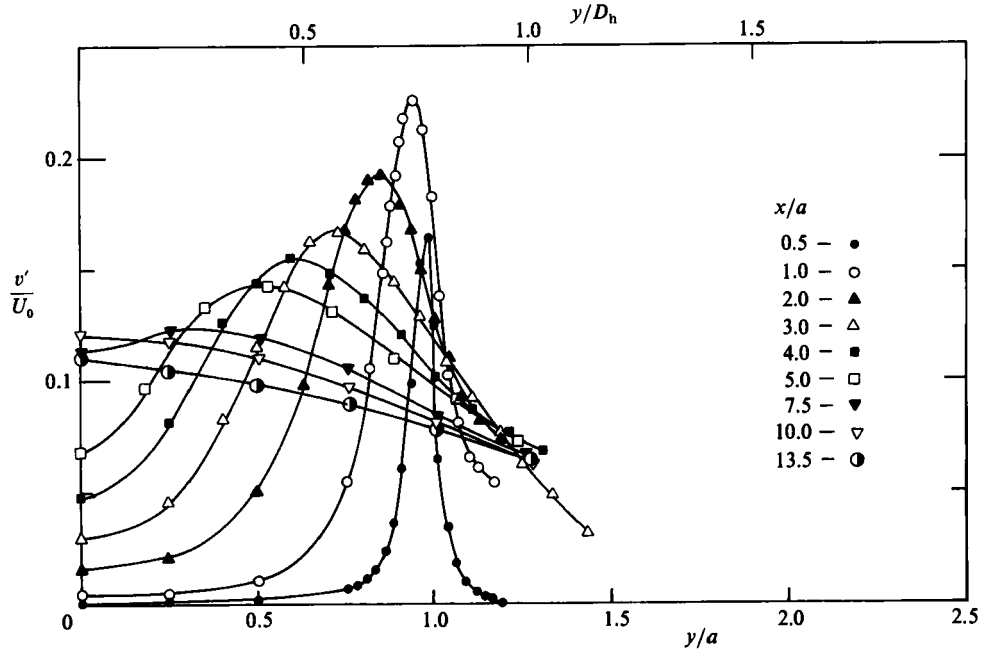

FIGURE 20. The v'-profiles in the major-axis plane.

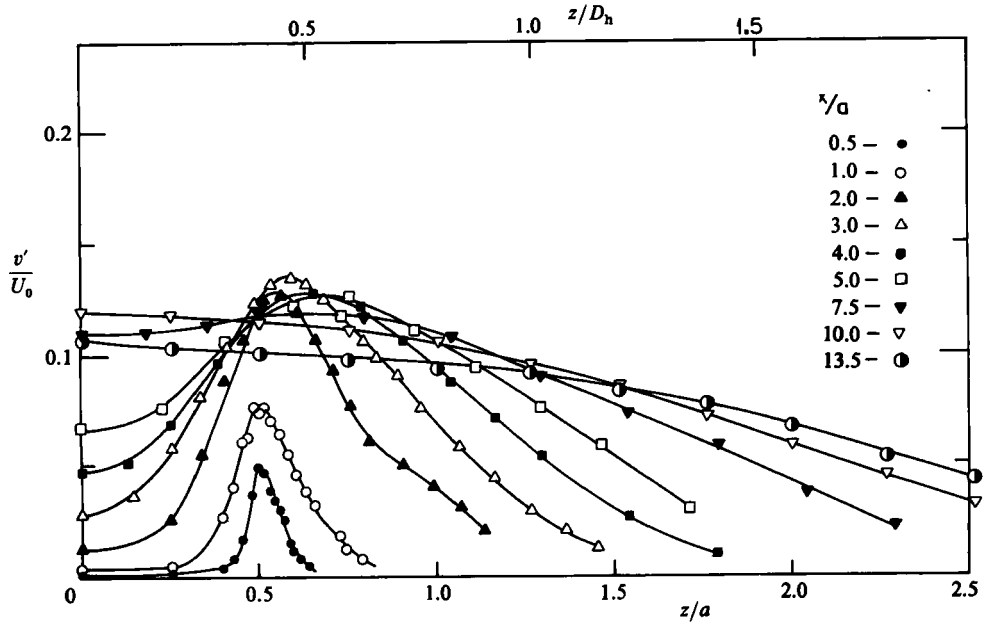

FIGURE 21. The v'-profiles in the minor-axis plane.

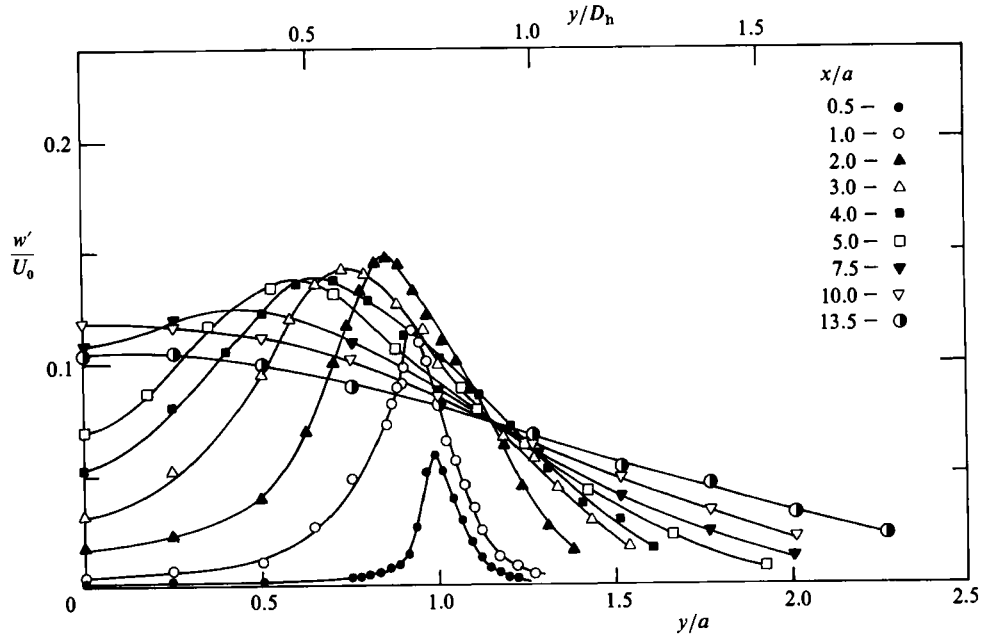

FIGURE 22. The w'-profiles in the major-axis plane.

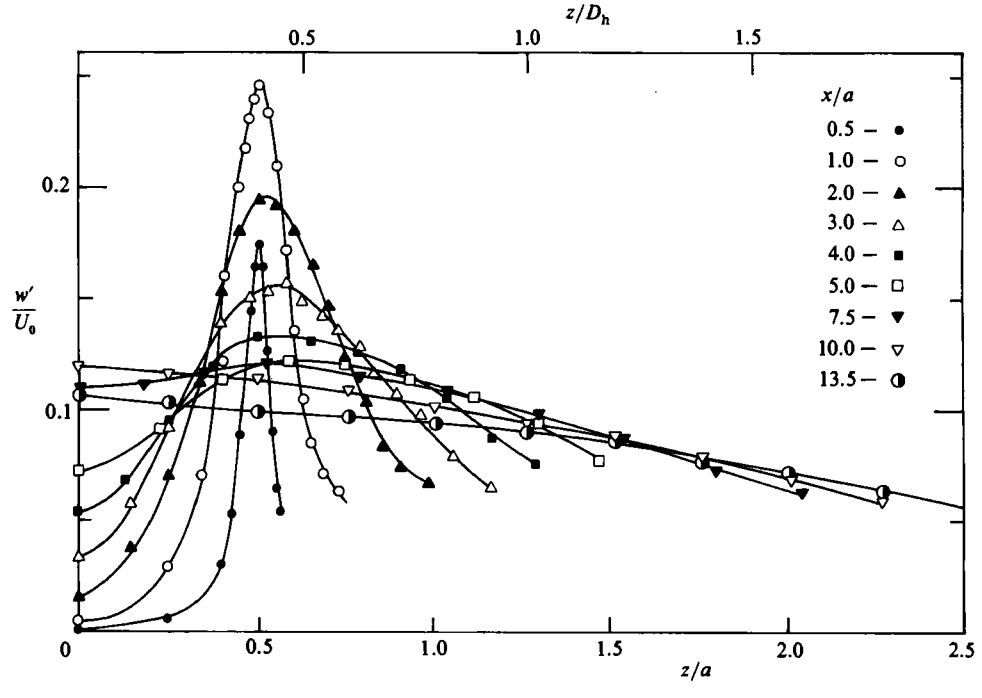

FIGURE 23. The w'-profiles in the minor-axis plane.

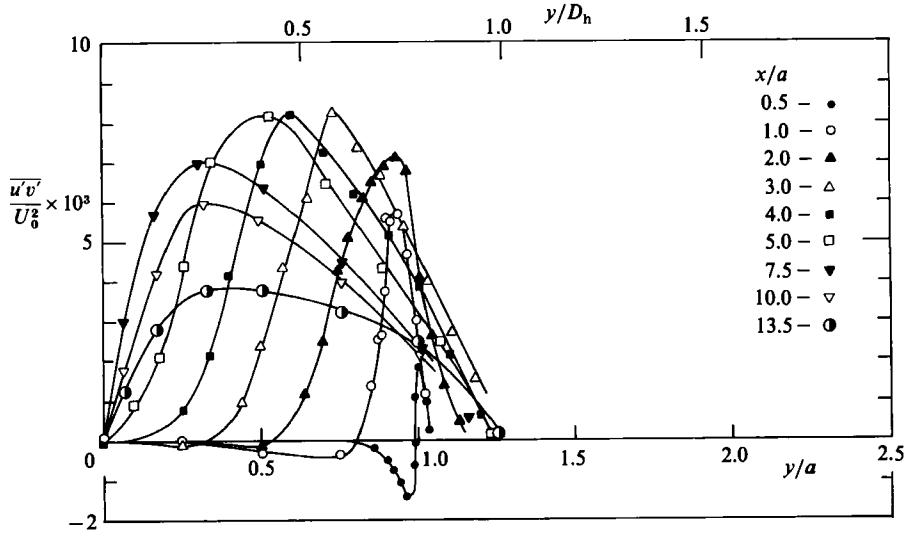

FIGURE 24. The $\overline{u'v'}$ profiles in the major-axis plane.

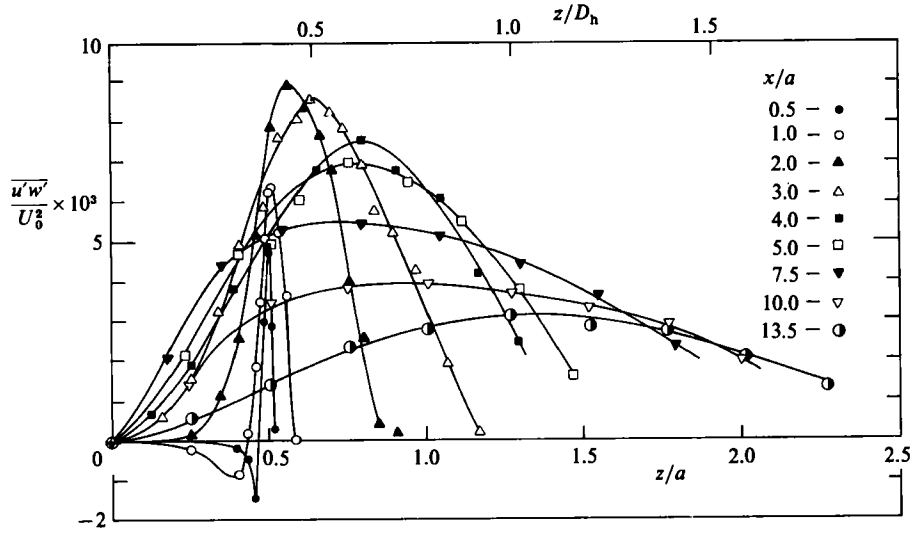

FIGURE 25. The $\overline{u'w'}$ profiles in the minor-axis plane.

perpendicular to the radial direction and in the direction of the mean vortex line. Their peak values occurred at $x = 2a$ to $3a$ and equalled about $0.15U_0$.

6.2. *Reynolds stress*

In the major-axis plane, the Reynolds stress $\overline{uv}$ was almost zero beyond $y/a \approx 1.25$ (figure 24). This shows that most of the transverse momentum transfer occurs in the high-speed region. The velocity fluctuations u' and v' (figures 18 and 20) were not correlated on the low-speed side, $y/a > 1.25$. On the other hand, the momentum transfer in the minor-axis plane mainly occurred beyond $y/a > 0.5$ where the elliptic vortex expanded outward.

Regions of negative Reynolds stress are detectable at $x/a = 0.6$ and 1.0 (figures 24 and 25). The negative Reynolds stress is associated with the negative production of turbulence (Oster & Wygnanski 1982) and can be explained by the vortex nutation idea (Browand & Ho 1983). It always happens in the non-pairing state of a single vortex or in the latter part of the vortex merging. In the present case, the first two vortex mergings occurred near $x/a = 0.6$ and 1.0 where the negative Reynolds stress was measured.

7. Conclusion

In an *unforced* elliptic jet with a small aspect ratio (2:1), the mass entrainment ratio is several times higher than that in a circular or a two-dimensional jet. *The physical mechanism of this phenomenal increase is the azimuthal distortion of the elliptic vortex caused by self-induction.* Most of the entrainment occurs around the minor-axis plane where the vortex core moves away from the jet axis and the external fluid is entrained into the jet stream. Thus, a *passive control* of the entrainment is achieved.

Owing to the self-induction of the vortex, axis switching occurs three times in the range of $x/a \leqslant 40$. The cross-section at $x/a = 40$ is almost but not quite circular. Because of the axis switching, the flow properties, mean velocity, turbulence intensities and Reynolds stress are very different in the major- and minor-axis planes. Self-similarity is not observed in the measuring range.

The initial momentum thicknesses in the major and minor axes have a difference of 26%, but there is only one independent instability frequency across the entire nozzle. From the available evidence, the thinnest momentum thickness seems to be the lengthscale for the instability because it associates with the maximum vorticity around the nozzle.

This work is supported under AFOSR Contract No. F49620-82-K-0019. The authors appreciate the help from Dr S. Koshigoe who provided us with the calculated eigenfunctions.

REFERENCES

Browand, F. K. & Ho, C.-M. 1983 The mixing layer: an example of quasi two-dimensional turbulence. *J. Mec. Theor. Appl.* (numero spécial) 99–120.

Crighton, D. G. 1974 Instability of an elliptic jet. *J. Fluid Mech.* **59**, 665–672.

Crow, S. C. & Champagne, F. H. 1971 Orderly structure in jet turbulence. *J. Fluid Mech.* **48**, 547–591.

Dhanak, M. R. & De Bernardinis, B. 1981 The evolution of an elliptic vortex ring. *J. Fluid Mech.* **109**, 189–216.

Gutmark, E. & Ho, C.-M. 1982 Development of an elliptical jet. *Bull. Am. Phys. Soc.* **27**, 1184.

Gutmark, E. & Ho, C.-M. 1983 On a forced elliptic jet. *Proc. 4th Turbulent Shear Flow Conf. Karlsruhe, Germany.* Springer.

Gutmark, E. & Ho, C.-M. 1985 Near field pressure fluctuations of an elliptical jet *AIAA J.* **23**, 345–358.

Gutmark, E. & Ho, C.-M. 1986 Visualization of a forced elliptic jet. *AIAA J.* **24**, 684–685.

Heskestad, G. 1965 Hot-wire measurements in a plane turbulent jet. *Trans. ASME* E: *J. Appl. Mech.* 721–734.

Ho, C.-M. & Gutmark, E. 1982 Visualization of an elliptical jet. *Bull. Am. Phys. Soc.* **27**, 1184.

Ho, C.-M. & Hsiao, F. B. 1982 Evolution of coherent structures in a lip jet. In *Structure of Complex Turbulent Shear Flow*, pp. 121–136. Springer.

Ho, C.-M. & Huang, L. S. 1982 Subharmonics and vortex merging in mixing layers. *J. Fluid Mech.* **119**, 443–473.

Ho, C.-M. & Huerre, P. 1984 Perturbed free shear layers. *Ann. Rev. Fluid Mech.* **16**, 365–424.

Husain, H. S. & Hussain, A. K. M. F. 1983 Controlled excitation of elliptic jets. *Phys. Fluids* **26**, 2763–2766.

Kibens, V. & Wlezien, R. W. 1985 Active control of jets from indeterminate origin nozzle. *AIAA Paper No.* 85-0542.

Komatsu, Y. 1969 Fluid dynamics of jets. *Internal Rep.*, Nippon University.

Koshigoe, S., Yang, V., Culick, F. E. C. & Tubis, A. 1986 A new method for stability analysis of a free jet with arbitrary cross section. *AIAA Paper No.* 86-0542.

Krothapalli, A., Baganoff, D. & Karamcheti, K. 1981 On the mixing of a rectangular jet. *J. Fluid Mech.* **107**, 201–220.

Lee, M. & Reynolds, W. C. 1985 Bifurcating and blooming jet. *Tech. Rep.* TF-22, Stanford University.

Michalke, A. 1965 On spatially growing disturbances in an inviscid shear layer. *J. Fluid Mech.* **23**, 521–544.

Michalke, A. & Hermann, G. 1982 On the inviscid instability of a circular jet with external flow. *J. Fluid Mech.* **114**, 345–359.

Monkewitz, P. A. & Huerre, P. 1982 The influence of the velocity ratio on the spatial instability of mixing layers. *Phys. Fluids* **25**, 1137–1143.

Morris, P. J. & Miller, D. G. 1984 Wavelike structures in elliptic jet. *AIAA Paper No.* 84-0399.

Oster, D. & Wygnanski, I. 1982 The forced mixing layer between parallel streams. *J. Fluid Mech.* **123**, 91–130.

Reynolds, W. C. & Bouchard, E. E. 1981 The effect of forcing on the mixing-layer region of a round jet. In *Unsteady Turbulent Shear Flows* (ed. R. Michel, J. Cousteix & R. Houdeville), pp. 402–411. Springer.

Schadow, K. C., Wilson, K. J., Lee, M. J. & Gutmark, E. 1984 Enhancement of mixing in ducted rockets with elliptic gas-generator nozzles. *AIAA Paper No.* 84-1260.

Sfeir, A. A. 1978 Investigation of three-dimensional turbulent rectangular jets. *AIAA J.* **16**, 1055–1060.

Sforza, P. M., Steiger, M. H. & Trentacoste, N. 1966 Studies on three-dimensional viscous jets. *AIAA J.* **4**, 800–806.

Trentacoste, N. & Sforza, P. 1967 Further experimental results for three-dimensional free jets. *AIAA J.* **5**, 885–891.

Viets, H. & Sforza, P. M. 1972 Dynamics of bilaterally symmetry vortex rings. *Phys. Fluids* **15**, 230–240.

Winant, C. D. & Browand, F. K. 1974 Vortex pairing: the mechanism of turbulent mixing layer growth at moderate Reynolds number. *J. Fluid Mech.* **63**, 237–255.

Wygnanski, I. & Fiedler, H. E. 1969 Some measurements in the self-preserving jet. *J. Fluid Mech.* **38**, 577–612.